scientific reports

Check for updates

OPEN

Evaluation study on gas-phase passivation inhibiting the spontaneous combustion tendency of ferrous sulfide compounds

Yuanyuan Zhang[1]✉, HaSung Kong[2]✉, Ruixuan Hao[3], Qin Xu[4] & Long Zhao[1]

The iron sulfide compound FeS, present in petrochemical plants, is prone to spontaneous combustion when exposed to air, posing a significant threat to the safety of production processes in the petrochemical industry. Accurately assessing the spontaneous combustion tendency of FeS is crucial for preventing fire and explosion hazards in petrochemical storage tanks. In this study, FeS was passivated with 3%, 6%, and 9% concentrations of passivator for 2 to 8 h, and the effects of gas-phase passivation on FeS were investigated. Thermodynamic and pore structure parameters were extracted through simultaneous thermal analysis and BET specific surface area measurement experiments. The entropy-weight TOPSIS method was then used to evaluate the passivated samples and determine the optimal passivation conditions. The results show that the entropy-weight method assigns dominant weights to the duration temperature in the room-temperature spontaneous combustion stage (ΔT_1, 10.2%) and the activation energy in the high-temperature combustion stage (E_3, 9.3%), indicating that the thermodynamic suppression effect, driven by the passivation mechanism, plays a more significant role than the changes in the microstructure. TOPSIS analysis reveals that the FeS sample passivated for 8 h with a 9% passivator concentration has the lowest spontaneous combustion tendency (composite score of 0.743), while the highest risk is associated with the sample passivated for 2 h with a 3% concentration (composite score of 0.341). The passivator concentration is positively correlated with inhibition efficiency, and selecting a gas-phase passivator concentration between 6% and 9%, with a passivation time of over 4 h, ensures higher safety and superior passivation effectiveness.

Keywords TOPSIS, Spontaneous combustion FeS, Gas-phase passivation, Inhibition effect, Comprehensive evaluation

During the process of petroleum storage and refining, active sulfur in crude oil corrodes the internal walls of equipment, forming ferric sulfide corrosion products primarily composed of FeS. These pyrite corrosion products exhibit strong oxidation and self-ignition activity. Under normal pressure and temperature conditions, they can spontaneously combust upon exposure to air, igniting flammable and explosive substances and potentially causing fire and explosion accidents[1–3]. To address the spontaneous combustion of FeS, current prevention and control methods mainly include isolation, cleaning, and passivation. In recent years, some scholars have conducted research on the passivation of iron sulfide compounds[4]. Liu et al.[5] demonstrated that ionic liquids could effectively inhibit the spontaneous combustion of iron sulfide compounds. After treatment, the surface roughness of iron sulfide increased, and the maximum weight loss temperature shifted toward the high-temperature zone. Molecular simulations revealed that imidazole ions competed with oxygen molecules for adsorption on FeS, thereby inhibiting their spontaneous combustion thermal behavior. However, in practical applications, the inhibitory effect and operability remain limited. Dou et al.[6] utilized a mixed gas with a limited oxygen concentration to suppress the spontaneous combustion of iron sulfide and proposed a suppression process for distillation towers. Gao et al.[7] found that deep vapor phase passivation promoted the conversion of the S element in FeS to SO_2, accelerated the formation of an oxide film on the FeS surface, and led to the

[1]School of Environmental and Safety Engineering, Liaoning Petrochemical University, Fushun 113001, China. [2]Department of Fire Disaster Prevention, Woosuk University, Wanju, Chonbuk 55338, Republic of Korea. [3]School of Safety Engineering, Beijing Institute of Petrochemical Technology, Beijing 102617, China. [4]School of Resources and Environmental Engineering, Shanghai Polytechnic University, Shanghai 201209, China. ✉email: zhangyuanyuan@lnpu.edu.cn; 119wsu@naver.com

expansion and swelling of internal pores. Xu et al.[8] treated active FeS with low-concentration passivator gas and observed that the self-ignition tendency weakened as passivation time extended. They recommended extending the passivation time to more than 6 h. Although these studies have made progress in mechanism exploration and process optimization, certain prevention and control measures still face limitations in practical engineering applications. While the isolation method can partially prevent FeS from contacting air, it is challenging to completely eliminate air intrusion caused by tiny gaps or leaks, and the maintenance cost remains relatively high. The cleaning method encounters difficulties in completely removing FeS due to the complex internal structure of equipment, often resulting in residues[9]. Moreover, the cleaning process generates substantial wastewater requiring subsequent treatment and increasing environmental protection costs[10]. Gas phase passivation technology, as a novel clean and environmentally friendly method, features high efficiency and low cost. This process involves converting sulfur-containing corrosion products such as FeS into stable compounds through gas passivators. The passivator reacts with active sites on the FeS surface, generating stable compounds across the entire outer surface of the particles, rendering them non-flammable and achieving a passivation effect[11]. By precisely controlling the concentration of the passivator and the passivation time, the gas-phase passivation method can more accurately suppress the self-ignition tendency of FeS, regulate the passivation effect, and provide flexibility for actual production[12,13].

Research on the passivation effects of methods for inhibiting pyrite compounds primarily focuses on single-factor influences or qualitative observations, lacking a systematic framework for quantitative evaluation. Currently, the self-ignition risk assessment of FeS relies on simple thermodynamic indicators or traditional logical analysis methods[14]. Shi et al.[15]quantitatively evaluated the risks of storage tank accidents by constructing a fault tree (FTA) and comprehensively assessed oil depot accidents by combining the expert heuristic improved Analytic Hierarchy Process (AHP) with fuzzy set theory. However, subjective deviations persist in weight assignment. Notably, multi-criteria decision-making methods such as TOPSIS have demonstrated strong applicability in industrial safety[16,17]. Aliya Fahmi et al.[18]took natural gas-related accidents as an example and established an evaluation model combining Bayes and TOPSIS; Nurdan Tuysuz et al.[19]proposed the image fuzzy Z-TOPSIS (PFZ-TOPSIS) method to comprehensively analyze the practicability and superiority of solar panels and solve selection problems. Zhu et al.[20] determined parameters such as pH and specific surface area of biochar using scanning electron microscopy and Fourier transform infrared spectroscopy, evaluating its application potential via the entropy weight TOPSIS method. However, the application of the TOPSIS method in FeS gas phase passivation has yet to be explored. By referring to the entropy weight method to reduce subjective deviations in weight allocation of evaluation indicators, an objective framework is provided for comprehensive parameter weighting, enabling effective evaluation of the inhibition effect of passivated samples[21].

This study systematically investigated the comprehensive effects of passivator concentrations (3%, 6%, 9%) and treatment times (2–8 h) on the reactivity of FeS. Through synchronous thermal analysis experiments and BET specific surface area measurement experiments, 25 thermodynamic and pore structure parameters were extracted to construct an entropy weight-TOPSIS evaluation model. Finally, the key indicators for controlling spontaneous combustion suppression and the optimal passivation conditions for the FeS reaction were determined. By integrating experimental characterization with data-driven decision analysis, actionable insights are provided for the safety maintenance practices of petrochemical facilities.

Materials and methods

Experimental process

The experimental procedure is schematically illustrated in Fig. 1. Active FeS samples were synthesized using sodium sulfide (AP, ≥98%) and ammonium ferrous sulfate (AP, ≥99.5%) as raw materials. The synthesized active FeS was vacuum-dried in a glove box to prevent oxidation, with the dried samples subsequently milled and partitioned in the same environment. In this paper, the passivation treatment of active FeS was carried out in terms of both duration and concentration, respectively. After the passivation treatment, the FeS particles underwent thermodynamic analysis and BET specific surface area measurements to determine characteristic parameters indicative of spontaneous combustion tendency. The correlation analysis of the extracted parameters was carried out. Finally, the characteristic parameters extracted from thermodynamic and BET specific surface area measurement were used as evaluation indexes for TOPSIS treatment of FeS treated with different passivation times and different passivation concentrations, and the optimal combination of passivation time and concentration was obtained to minimize the spontaneous combustion tendency of Active FeS after passivation.

The FeS gas-phase passivation device primarily comprises a passivation reactor, a monitoring system, a gas supply unit, and a tail gas treatment module. Screened active FeS powder is loaded into the passivation reactor, where passivation is performed using gas-phase passivation agents at concentrations of 3%, 6%, and 9% (a mixture of nitrogen and oxygen, corresponding to oxygen volume fractions of 3%, 6%, and 9%)[7]. The gas flow rate is set at 10 ml/min. For each concentration of the gas-phase passivator, passivation is conducted for durations of 2, 4, 6, and 8 h, respectively. All sampling procedures must be performed under air-free conditions within a vacuum glove box to ensure isolation from ambient air. The active and gas-phase passivated samples are subsequently sealed with specialized sealing films and stored in a controlled environment. During the gas-phase passivation process, the exhaust gas is directed through a ventilation hood to prevent potential damage to equipment and ensure personnel safety. The passivation procedure for active FeS is illustrated in Fig. 2. Active FeS is dried and ground to a particle size range of 110–160 mesh prior to its use in subsequent passivation steps. Gas-phase passivation is carried out at 25℃ under normal pressure conditions. A total of twelve passivated sample groups are obtained based on varying concentrations and exposure times. Unpassivated active FeS samples are designated as A0, while the numbering of passivated samples is detailed in Table 1.

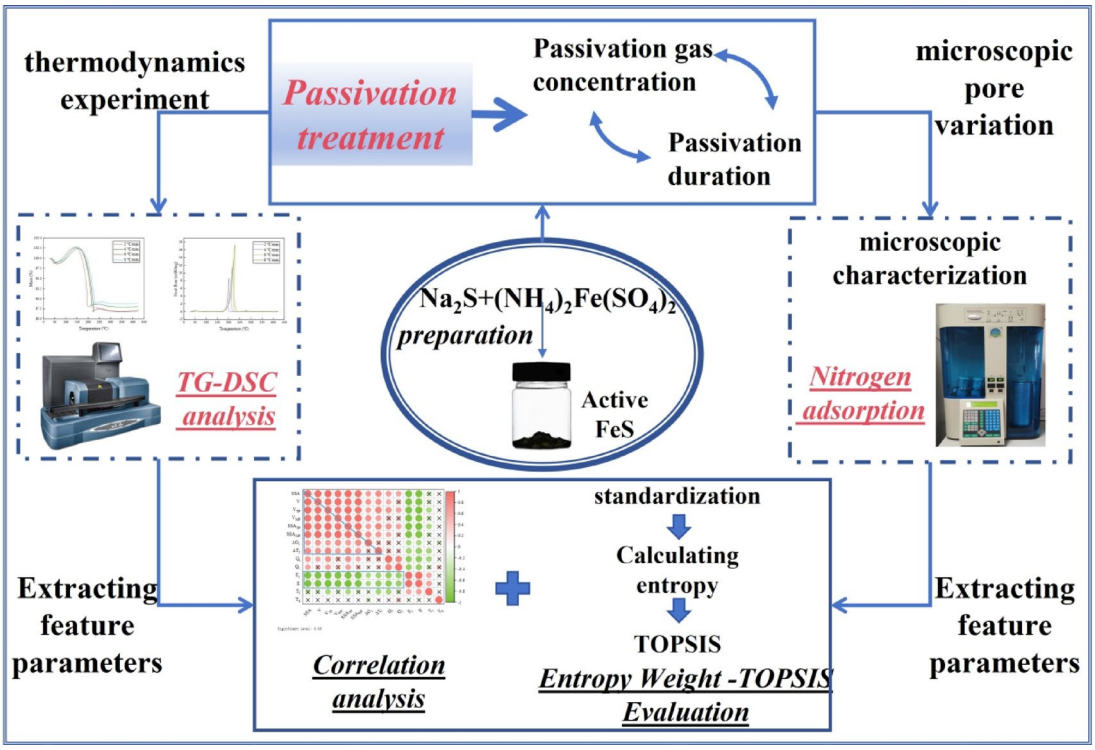

Fig. 1. Experimental flow chart.

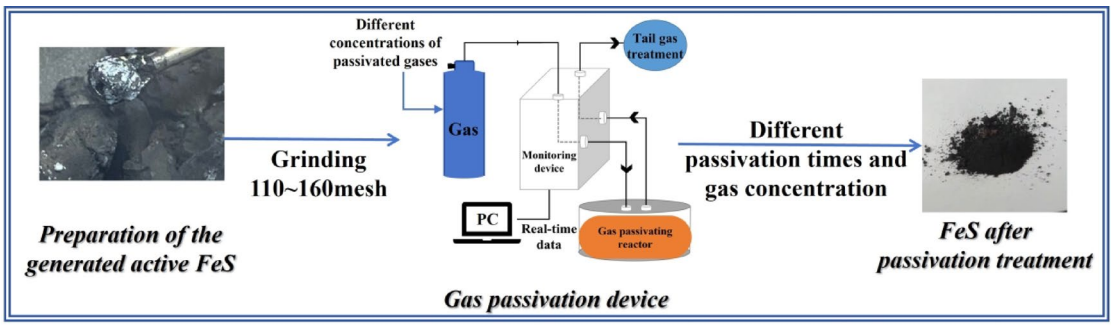

Fig. 2. Passivation flow chart.

Experimental instruments

Thermogravimetric analysis was conducted using the SDT-Q600 simultaneous thermal analyzer (TA Instruments, USA). The experimental conditions were set as follows: dry air atmosphere with a gas flow rate of 50 mL/min; temperature range from room temperature (RT) to 400 °C; heating rates of 5, 10, 15, and 20 °C/min. Thermogravimetric (TG) and differential scanning calorimetry (DSC) data for samples under different passivation conditions were obtained across these heating rates.

Pore structure characterization of active and passivated FeS was performed using a NOVA 2000e fully automatic specific surface area and pore size distribution analyzer (Quantachrome, USA). This instrument features four analysis stations and four degassing stations, with a relative pressure (P/P_0) measurement range of 0.001–0.998. Repeatability accuracy for pore size and specific surface area is 0.02 nm and 1%, respectively. Following degassing and weighing, FeS samples were analyzed using high-purity N_2 (99.999%) as the adsorbate at 77 K. Measurements covered a relative pressure range of 0.05–0.95, with data points collected at 0.05 intervals. Direct air exposure of FeS was prevented throughout the procedure. Nitrogen adsorption isotherms were used to calculate pore parameters via the BJH (Barrett-Joyner-Halenda) and BET (Brunauer-Emmett-Teller) methods.

Surface morphology and compositional analysis were performed using an FEI Quanta 400 field emission scanning electron microscope (FEI, USA). Sample imaging employed secondary electron detection, with qualitative and quantitative microanalysis conducted using backscattered electron imaging and X-ray energy dispersive spectroscopy (EDS, model APEX, EDAX Inc., USA). Prior to analysis, samples were mounted on aluminum stubs and coated with a ~ 5 nm layer of gold via sputter coating to enhance electrical conductivity.

Number	Passivation concentration	Passivation time	
-	%	hours	Acronyms
1	3	2	B2
2		4	B4
3		6	B6
4		8	B8
5	6	2	C2
6		4	C4
7		6	C6
8		8	C8
9	9	2	D2
10		4	D4
11		6	D6
12		8	D8

Table 1. Passivation sample number.

Entropy weights and TOPSIS evaluation methods

Entropy weighting

The Entropy Weight Method, rooted in the concept of information entropy, determines the weight of each indicator by calculating its entropy value. Herein, entropy serves as a measure of uncertainty: the greater the entropy value of an indicator, the smaller its assigned weight. This approach mitigates the ambiguity of subjective weight assignment, rendering the weight-determination process more objective and scientifically rigorous[18].

Step 1: It is assumed that the original matrix X consists of m samples, n indicators, which together form the matrix $X=(X_{ij})_{m*n}$. where the samples are 12 sets of passivation samples with different passivation parameters, and the evaluation indicators are the parameters in the thermodynamic and pore parameters of the BET specific surface area measurement experiment

$$X = \begin{Bmatrix} x_{11} & x_{12} & \cdots & x_{1n} \\ x_{21} & x_{22} & \cdots & x_{2n} \\ \vdots & \vdots & \ddots & \vdots \\ x_{m1} & x_{m2} & \cdots & x_{mn} \end{Bmatrix}_{m*n} \tag{1}$$

Step 2: The raw data are standardized according to the standardization formula to ensure that there is no quantitative gap between the indicators, and the values of the raw data are set between [0,1]. There are four cases of forwarding treatment in the evaluation indicators, namely: forward indicators, reverse indicators, intermediate indicators and interval indicators. Among them, this paper deals with the forward normalization treatment of forward and reverse indicators[22,23].

Positive indicators are indicators whose larger value is more favorable to the evaluation object, such as activation energy (E) in this paper. The normalization formula for positive indicators is as follows:

$$x_{ij}^{+} = \frac{x_{ij} - \min(x_{1j}, \ldots\ldots, x_{mj})}{\max(x_{1j}, \ldots\ldots, x_{mj}) - \min(x_{1j}, \ldots\ldots, x_{mj})} \tag{2}$$

Negative indicators are indicators whose larger value is more favorable to the evaluation object, such as Heat release (Q) in this paper. The normalization formula for positive indicators is as follows:

$$x_{ij}^{-} = \frac{\max(x_{1j}, \ldots\ldots, x_{mj}) - x_{ij}}{\max(x_{1j}, \ldots\ldots, x_{mj}) - \min(x_{1j}, \ldots\ldots, x_{mj})} \tag{3}$$

The values of the indicators that have been normalized according to Eq. (2) (3) form the matrix X^1.

$$X^1 = \begin{Bmatrix} x_{11}^1 & x_{12}^1 & \cdots & x_{1n}^1 \\ x_{21}^1 & x_{22}^1 & \cdots & x_{2n}^1 \\ \vdots & \vdots & \ddots & \vdots \\ x_{m1}^1 & x_{m2}^1 & \cdots & x_{mn}^1 \end{Bmatrix}_{m*n} \tag{4}$$

Step 3: After normalizing each evaluation indicator, the information entropy of the evaluation indicator is obtained according to Eq. (5), and the utility value of the evaluation indicator can be obtained from Eq. (6).

$$e_j = -k \sum_{i=1}^{m} p_{ij} \ln(p_{ij}) \tag{5}$$

$$d_j = 1 - e_j \tag{6}$$

where, e_j is the information entropy; $k = 1/lnm$; $p_{ij} = \frac{x_{ij}^1}{\sum_{i=1}^{m} x_{ij}^1}$ is the weight of the normalized value, representing the proportion of the -th sample in the -th index: ; d_j is the information utility value.

Step 4: Finally, the objective weights of the evaluation indicators ω_j are determined according to Eq. (7).

$$\omega_j = \frac{d_j}{\sum_{j=1}^{n} d_j} \tag{7}$$

The calculated weight values of the different evaluation indicators can be used for the next step of TOPSIS evaluation.

TOPSIS

As a widely adopted methodology for multi-criteria decision-making, TOPSIS (Technique for Order of Preference by Similarity to Ideal Solution) effectively leverages raw data to generate results that precisely reflect the disparities among evaluation alternatives[24]. The methodology typically proceeds as follows: first, the raw data matrix is normalized to eliminate dimensional discrepancies; second, cosine similarity is employed to identify the ideal (best) and anti-ideal (worst) solutions within the candidate set. Subsequently, Euclidean distances from each evaluation object to both the ideal and anti-ideal solutions are computed. Finally, the relative closeness of each object to the ideal solution—defined as the ratio of its distance to the anti-ideal solution over the sum of distances to both solutions—serves as the quantitative criterion for ranking their performance[25].

Step 1: The matrix X^1 formed from the normalization of the original matrix X, is shown in Eq. (4).

Step 2: As shown in Eq. (8) for constructing the weighted normalized matrix.

$$Z = \omega_j \begin{Bmatrix} x_{11}^1 & x_{12}^1 & \cdots & x_{1n}^1 \\ x_{21}^1 & x_{22}^1 & \cdots & x_{2n}^1 \\ \vdots & \vdots & \ddots & \vdots \\ x_{m1}^1 & x_{m2}^1 & \cdots & x_{mn}^1 \end{Bmatrix}_{m*n} \tag{8}$$

where ω_j is the weight value calculated by the entropy weighting method, $\omega=(\omega_1,\omega_2, \ldots, \omega_n)^T$.

Step 3: The positive ideal solution Z^- and the negative ideal solution Z^+ can be obtained through Eqs. (9) and (10).

$$Z^+ = (\max Z_{i1}, \max Z_{i2}, \ldots, \max Z_{in}) \tag{9}$$

$$Z^- = (\min Z_{i1}, \min Z_{i2}, \ldots, \min Z_{in}) \tag{10}$$

where max Z_{ij} is the maximum value of the '*j*' evaluation indicator for all evaluation objects; minZ_{in} is the minimum value of the '*j*' evaluation indicator for all evaluation objects.

Step 4: The distance between the ideal solution and the evaluation object can be determined from Eqs. (11) and (12).

$$D_i^+ = \sqrt{(\max Z_{ij} - Z_{ij})^2} \tag{11}$$

$$D_i^- = \sqrt{(\min Z_{ij} - Z_{ij})^2} \tag{12}$$

Step 5: The proximity C_i of the ideal solution to the evaluation object is determined according to Eq. (13), and the evaluation results are derived from the magnitude of C_i and thus the evaluation results.

$$C_i = \frac{D_i^-}{D_i^+ + D_i^-} \tag{13}$$

The above steps lead to the result of evaluating the spontaneous combustion tendency of passivated FeS: the proximity C_i value. When the proximity is high, it indicates that the spontaneous combustion tendency of the evaluated object is low, the better the passivated sample is passivated, no spontaneous combustion occurs at room temperature, and the safety is higher. When the proximity is closer to 0, the sample has a high tendency to spontaneous combustion and is more dangerous[26].

Experiment results and discussion

Simultaneous thermal analysis experiments and thermodynamic analysis

The thermogravimetric and heat flow curves of different FeS samples can be obtained by simultaneous thermal analysis experiments. As depicted in Fig. 3, the schematic TG curve of FeS sample D2 (9%-2 h) under a dry air atmosphere with a flow rate of 50 mL/min was obtained at a rate of 10 °C/min. According to the spontaneous combustion characteristics of FeS, the whole process can be divided into four stages, Stage I- spontaneous combustion at RT, Stage II-oxygen adsorption and weight gain stage, Stage III-high temperature combustion stage, and Stage IV- Burnout stage. The characteristic parameters for the characteristic stages of spontaneous

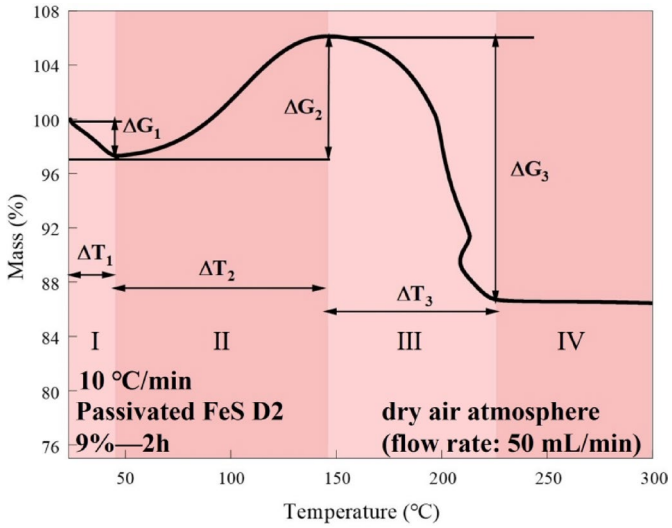

Fig. 3. TG curve of FeS sample D2 (9% passivator, 2 h) showing characteristic stages of spontaneous combustion.

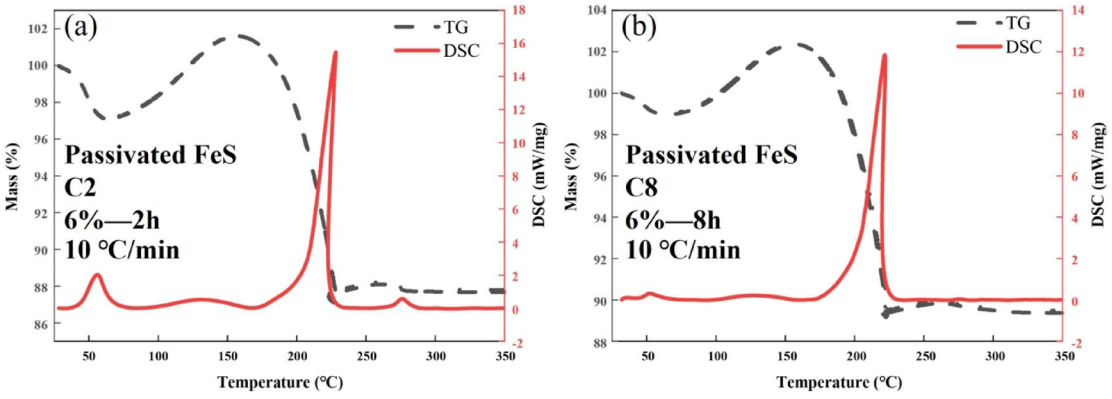

Fig. 4. TG-DSC curves of FeS samples C2 (6%-2 h) and C8 (6%-8 h) under dry air (50 mL/min, 10 °C/min). (**a**) FeS treated with 6% passivator for 2 h (C2). (**b**) FeS treated with 6% passivator for 8 h (C8).

combustion are shown below, with weight loss in Stage I denoted as ΔG_1 and sustained temperature denoted as ΔT_1, and oxygen uptake in Stage II denoted as ΔG_2 and sustained temperature denoted as ΔT_2. High temperature combustion in Stage III is denoted as ΔG_3 and sustained temperature denoted as ΔT_3.

Thermogravimetric and heat flow curve analysis

Figure 4 displays the TG-DSC curves of passivated samples C2 (a) and C8 (b). As the passivation time increases, the amount of FeS lost in the stage I decreases, and the peak value of the heat flow also decreases. When the passivation time reaches 8 h, the exothermic peak generated by FeS in the first stage basically disappears. As the passivation time increases, the amount of oxygen uptake increases, leading to a prolonged duration temperature into the high temperature combustion phase. The passivated FeS burns rapidly during the high temperature combustion phase, while the exothermic amount increases rapidly to reach the peak. The exothermic amount of the 2 h passivated sample is higher than that of the 8 h passivated sample. The longer the passivation time, the stronger the inhibition of spontaneous combustion of FeS.

Figure 5 depicts the TG-DSC profiles of passivated FeS samples B8(a) and D8(b). Prolonged passivation duration significantly diminished the Stage I exothermic peak intensity and reduced mass loss. At 8 h of passivation, both samples exhibited minimal exothermic activity in Stage I, accompanied by progressively flattened thermal profiles as passivator concentration increased. Oxygen absorption decreased with higher passivation concentrations: B4 showed about 6% mass gain, whereas D4 displayed negligible weight gain. After

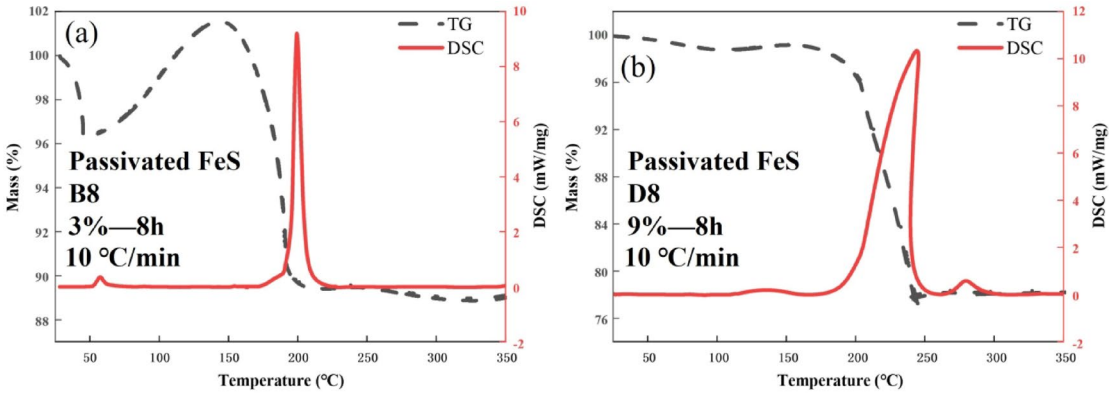

Fig. 5. TG-DSC curves of FeS samples B8 (3%-8 h) and D8 (9%-8 h) under dry air (50 mL/min, 10 °C/min). (**a**) FeS treated with 3% passivator for 8 h (B8). (**b**) FeS treated with 9% passivator for 8 h (D8).

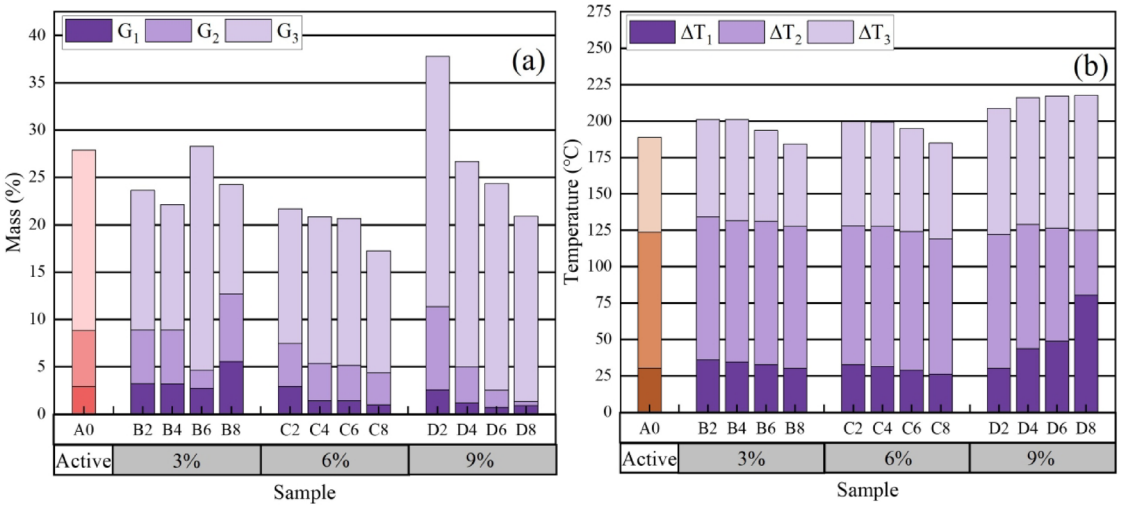

Fig. 6. The mean values of the mass change (a) and sustained temperature (b) of FeS during stage I-III with four heating rates (5, 10, 15, and 20 °C/min). Experimental conditions: Dry air (50 mL/min). (**a**) ΔG_1, ΔG_2, and ΔG_3 represent the mass changes (weight loss/weight gain) in stages I, II, and III, respectively. (**b**) ΔT_1, ΔT_2, and ΔT_3 are the sustained temperatures of the corresponding stages respectively.

the high temperature combustion phase, B4 exotherms up to 9 mW/mg, C4 about 12 mW/mg, while D4 reaches about 10 mW/mg. Increasing passivation duration and increasing passivator concentration more strongly inhibit the spontaneous combustion properties of FeS at the beginning of the spontaneous combustion process. During the high temperature combustion stage, the FeS with weaker passivation inhibition effect already undergoes partial exothermic behaviors in the early stage, resulting in the transfer of the exothermic behaviors of the FeS with stronger passivation effect to the later stage.

The variation in gas-phase passivation parameters directly influences the characteristic parameters of passivated FeS during the key stages of spontaneous combustion. As presented in Fig. 6, the mean values of the mass change (a) and sustained temperature (b) of FeS during Stages I - III under four heating rates (5, 10, 15, and 20 °C/min) are displayed. In Stage I, the lower weight loss associated with spontaneous combustion indicates a reduced propensity for spontaneous combustion. The increase in ΔT1 is primarily attributed to the enhancement of gas-phase passivation strength, which slows down the reaction process of passivated FeS in the first stage. In Stage II, lower oxygen absorption and shorter oxygen absorption time reflect a diminished oxygen absorption capacity, confirming the reduction of FeS active sites following passivation treatment, which significantly weakens its oxygen absorption capability. For Stage III, ΔG3 represents the mass change from the peak of oxygen absorption to the burnout stage. The mass change during the high-temperature combustion phase should be calculated from the point of maximum oxygen absorption. However, ΔT3 does not exhibit a clear trend. Throughout the entire combustion process, it is observed that the sample has a short duration in the first two characteristic stages, while the duration of the third stage is prolonged. This is due to the phenomena of spontaneous combustion weight loss and oxygen absorption weight gain in Stages I and II. Additionally, various complex substances form in the passivated sample as it enters Stage III, making the mass change during

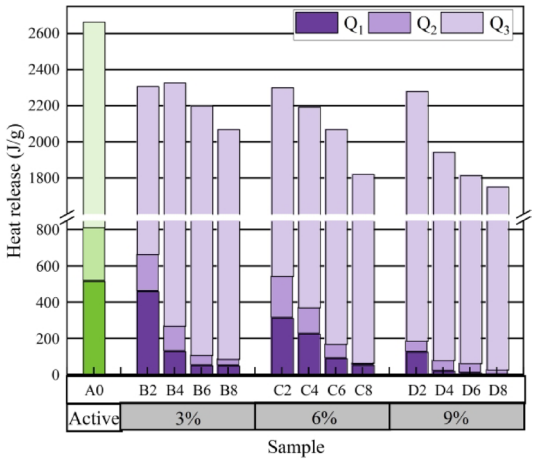

Fig. 7. The mean values of the Heat release(Q) of FeS during stage I-III with four heating rates (5, 10, 15, and 20 °C/min). Experimental conditions: Dry air (50 mL/min).

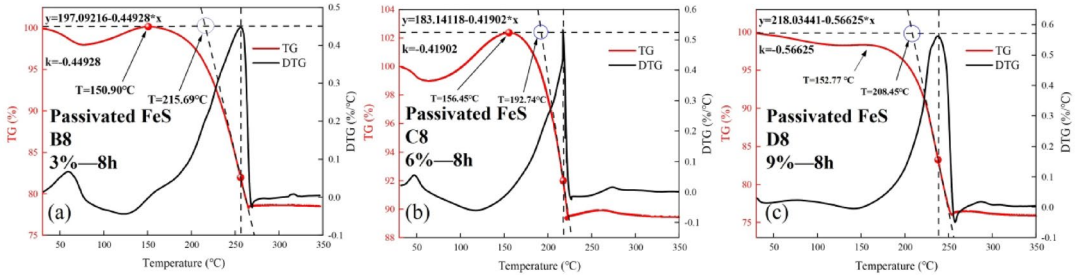

Fig. 8. Ignition temperature (T_I) and self-heating temperature (T_S) of FeS samples B8 (3%-8 h), C8 (6%-8 h), and D8 (9%-8 h) under dry air (50 mL/min, 20 °C/min). (**a**) B8 (3% passivator, 8 h): T_I = 215.69 °C, T_S = 150.90 °C. (**b**) C8 (6% passivator, 8 h): T_I = 192.74 °C, T_S = 156.45 °C. (**c**) D8 (9% passivator, 8 h): T_I = 208.45 °C, T_S = 152.77 °C.

combustion less precise. Nevertheless, if the enhanced passivation strength reduces the sample's spontaneous combustion tendency, the substances consumed during the first two stages will burn off in the third stage.

The analysis of the specific characteristic parameters in the TG curve offers a relatively simplistic evaluation of the gas-phase passivation effect. For a more comprehensive assessment, a combination of additional characteristic parameters should be considered in subsequent analysis and evaluation.

The exothermic values can be directly obtained by integrating the exothermic curves. As shown in Fig. 7, which presents the mean values of the Heat release of FeS during stage I-III with four heating rates (5, 10, 15, and 20 °C/min). The exothermic values released by A0 in Stages I and II are significantly higher than those of passivated FeS. The passivated samples emit considerably less heat at the onset of spontaneous combustion, indicating a much lower propensity for spontaneous combustion. Comparing the exothermic amount of high temperature combustion stage, B2, C2, C4, C8, D4, D6 and D8 are lower than the active FeS, which can be seen that with the deepening of the degree of gas-phase passivation, the spontaneous combustion of FeS is inhibited by the slowing down of the inhibition effect, and the exothermic amount of FeS continues to decrease, but the decrease rate is obviously smaller than that of the reduction of Stage I and II.

It is also essential to extract the ignition temperature and self-heating temperature from the TG curves during the spontaneous combustion of FeS. Figure 8 illustrates the ignition temperature (T_a) and self-heating temperature (T_s) of FeS samples that underwent an 8-hour passivation process: B8 (3%-8 h), C8 (6%-8 h), and D8 (9%-8 h). The experiments were carried out in a dry air environment (50 mL/min) with a heating rate of 20 ℃/min. In Stage III, the peak of the DTG curve corresponds to the point of maximum weight loss rate for FeS. The temperature at the intersection of the TG tangent at this peak and the maximum mass of the TG curve represents the ignition temperature of the sample. The ignition temperature is defined as the transition temperature at which a substance shifts from self-heating to spontaneous combustion[27]. The ignition temperatures for B8, C8, and D8 were 215.69 °C, 192.74 °C, and 208.45 °C, respectively. The decrease in oxygen absorption and duration temperature during the oxygen absorption and weight gain stage of passivated FeS results in a slower overall process. Consequently, the temperature required to reach the ignition point is delayed compared to that of active FeS. An increase in the ignition temperature indicates a stronger gas-phase passivation effect. The variation in self-heating temperature follows a trend similar to that of the ignition temperature, with a higher self-

heating temperature also signifying better gas-phase passivation. In addition to the characteristic parameters observed from the curves of the spontaneous combustion process, the activation energy calculated through thermodynamic methods can also be used as a valuable metric for evaluation.

Activation energy calculation

The activation energy represents the ease with which a reaction can take place and can be used as an evaluation indicator to determine the degree of a substance's propensity for spontaneous combustion[28]. In this paper, the FWO method of the non-conversion rate method is used to calculate E for FeS at different degrees of gas-phase passivation. The FWO method is expressed as:

$$G(\alpha) = \frac{A}{\beta}\int_0^T e^{-E/RT}dT \tag{14}$$

$$\lg\beta = \lg(\frac{AE}{RG(\alpha)}) - 2.315 - 0.4567\frac{E}{RT} \tag{15}$$

where E is the activation energy, J/mol; β is the rate of temperature increase, K/min; A is the finger-forward factor, s^{-1}; R is the gas constant, 8.3145 J/(mol·K); T is the peak temperature corresponding to the heating rate β, K.

Curve fitting was carried out based on the data at four different heating rates, and the slopes and intercepts of the fitted curves at different conversion rates were used to find the E and the Pre - exponential factor A for all the samples at different conversion rates. The fitted curve of 1/T versus Lgβ for A0 at Stage I is shown in Fig. 9.

As presented in Fig. 10, the mean values of the Activation energyof FeS during Stages I-III under four heating rates (5, 10, 15, and 20 °C/min) are displayed. The activation energies for Stage I, Stage II, and Stage III are denoted as E_1, E_2, and E_3, respectively. With the exception of E2 for B2, the activation energies (E_1, E_2, and E_3) of all other passivated FeS samples are higher than that of A0. The activation energy (E_3 = 223.86 kJ/mol) of FeS treated with 9% concentration for 8 h (D8) in the high-temperature combustion stage is 39% higher than that of FeS treated with 3% concentration for 2 h (B2) (E_3 = 161.23 kJ/mol). High-concentration and long-term passivation significantly enhances the reaction energy barrier. An increase in activation energy signifies that more energy is required for the reaction to occur, thus elevating the energy needed to drive the system and indicating that gas-phase passivation inhibits the spontaneous combustion of FeS.

Sample B2 may be insufficiently passivated, which leads to the exposure of active sites inside the FeS particles. This results in a slight increase in oxygen adsorption capacity during Stage II. However, as the degree of passivation deepens, the activation energy of passivated FeS increases significantly. While the apparent activation energy does not directly or accurately reflect the full extent of the gas-phase passivation effect, it can still serve as a useful metric for a comprehensive evaluation of the passivation effect[3,27].

Pore parameter analysis

BET specific surface area measurements of active and passivated FeS were performed using a fully automated specific surface area and pore size distribution meter. The pore parameters of the samples were determined by selecting an appropriate pore calculation method[29]. The adsorption isotherms of N_2(g) at liquid nitrogen temperature (77 K) and atmospheric pressure of active FeS are shown in Fig. 11. According to standard classification, the adsorption isotherm of FeS is identified as type IV, with the pore morphology primarily consisting of conical pores. From the desorption curve, it can be seen that the passivated FeS showed a hysteresis phenomenon, but in general the hysteresis return line was above the adsorption line, and the separation gap was not significant. The changes in pore shape and pore depth of FeS treated with different gas-phase passivator

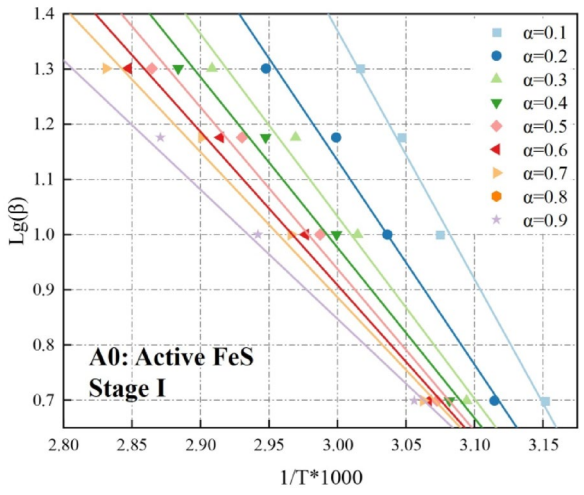

Fig. 9. Activation energy fitting curve for A0(active FeS) at Stage I.

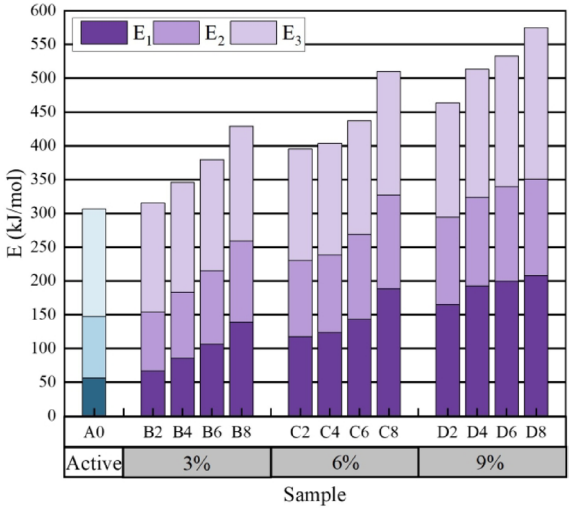

Fig. 10. The mean values of the Activation energy (E) of FeS during stage I-III with four heating rates (5, 10, 15, and 20 °C/min). Experimental conditions: Dry air (50 mL/min).

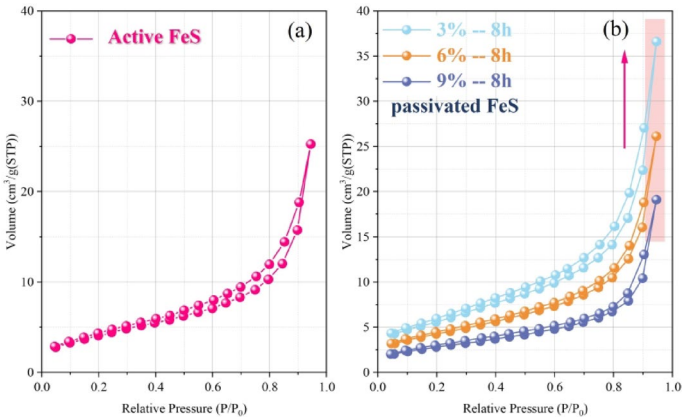

Fig. 11. FeS adsorption isotherms curves of N_2(g) at liquid nitrogen temperature (77 K) and atmospheric pressure.

concentrations and passivation times are prominent. The roughness of the surface of the pore material, and the complexity of the pores were significantly affected. While the adsorption and desorption curves of passivated FeS are similar to those of active FeS, there is a marked reduction in adsorption capacity. Specific parameters such as the specific surface area and pore size distribution of the samples were calculated from the liquid nitrogen adsorption data, using the BJH and BET methods. These parameters can then be used for subsequent comprehensive evaluation[30,31].

Pore volume and specific surface area analysis

The changes in surface porosity of the samples are directly observed through SEM. As shown in Fig. 12, the SEM images of FeS clearly reveal the changes in surface porosity characteristics after gas-phase passivation. Initially, the surface contains numerous pores with significant spatial separation. However, after gas-phase passivation, the surface and spatial morphology of FeS become more orderly and exhibit a more pronounced aggregation phenomenon, leading to a rapid evolution of the pore characteristics. Therefore, it is essential to study these changes in conjunction with the calculation methods for porosity characteristic parameters.

The pore volume and surface area of the samples can be calculated using the BJH method. Additionally, the pore structure of FeS was further categorized based on pore size, specifically micropores (< 10 nm) and transition pores (10–100 nm), to better analyze the pore characteristics of different types of FeS[32]. The total pore volume and total specific surface area of FeS are shown in Fig. 13. During the gas-phase passivation treatment, both the total pore volume and specific surface area of active FeS initially increase with the onset of passivation. However, after treatment with higher concentrations of passivator, both the pore volume and specific surface area decrease significantly. With longer passivation times, the total pore volume and surface area of FeS treated with the same gas-phase passivator concentration fluctuate in stages, reaching a minimum after 6–8 h. For FeS treated with

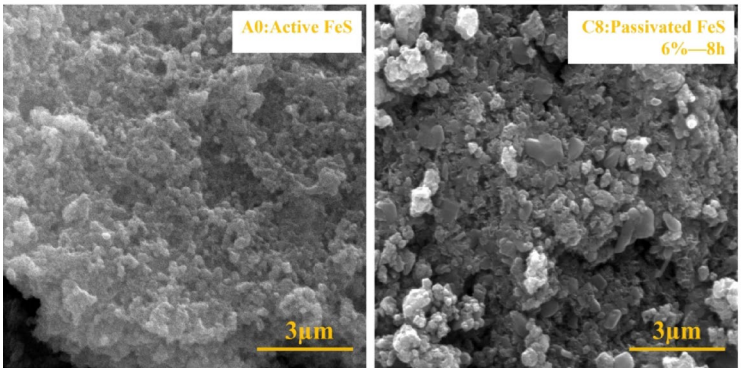

Fig. 12. The SEM images of A0(active FeS) and C8(6% passivator, 8 h).

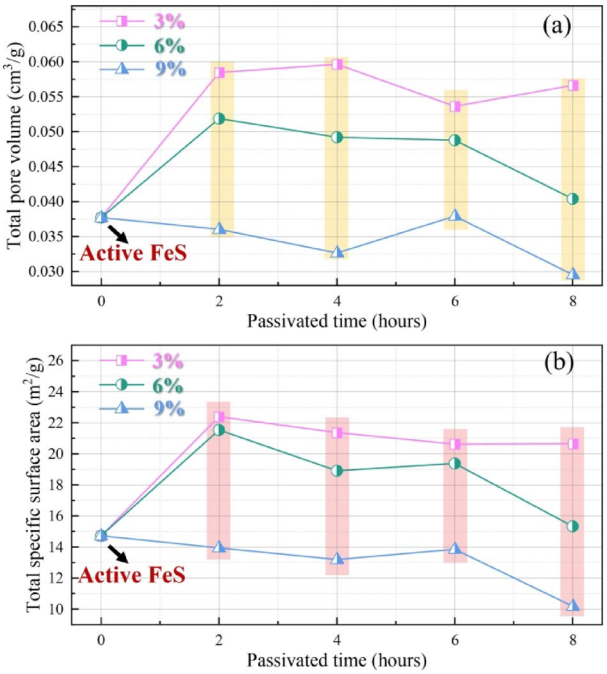

Fig. 13. Total pore volume (**a**) and total specific surface area (**b**) of FeS.

the same gas-phase passivator concentration, the total pore volume and specific surface area increase initially, but for FeS treated with a higher passivator concentration (9%), these values are smaller than those of active FeS. This indicates that gas-phase passivation effectively reduces the internal pore space and surface area of FeS, limiting its ability to react with sufficient oxygen molecules, thereby significantly inhibiting its spontaneous combustion activity. When the passivator concentration increased from 3 to 9% (with an 8 h treatment), the total pore volume of FeS decreased from 0.057 cm^3/g to 0.030 cm^3/g, and the specific surface area decreased from 20.65 m^2/g to 10.18 m^2/g. High-concentration passivator inhibits oxygen diffusion by filling micropores and reducing pore size (average pore diameter increased from 10.97 nm to 11.60 nm).

The pore variation characteristics can be further analyzed by the change rate and growth rate of pore volume and pore area under the variation of pore diameter. As shown in Fig. 14, it is the pore volume-pore diameter and pore specific surface area-pore diameter distribution diagrams of active FeS and FeS passivated for 8 h under different passivation concentrations. The cumulative total pore volume of active FeS reached 0.035 cm^3/g. The cumulative pore volume of passivated FeS changed significantly compared with that of active FeS. From the curves of pore volume and pore area varying with pore diameter, it can be found that under the same gas-phase passivation time conditions, as the concentration of gas-phase passivator increases, the pore volume and specific surface area of micropores and transition pores also show a decreasing trend. After passivation with a concentration of 9% gas-phase passivator for 8 h, the cumulative pore volume of FeS decreased by approximately 0.0073cm^3/g, which was approximately 20.92% lower than that of active FeS. The passivation effect is stronger with higher gas-phase passivator concentrations (9%), and prolonged passivation time slightly reduces the peak

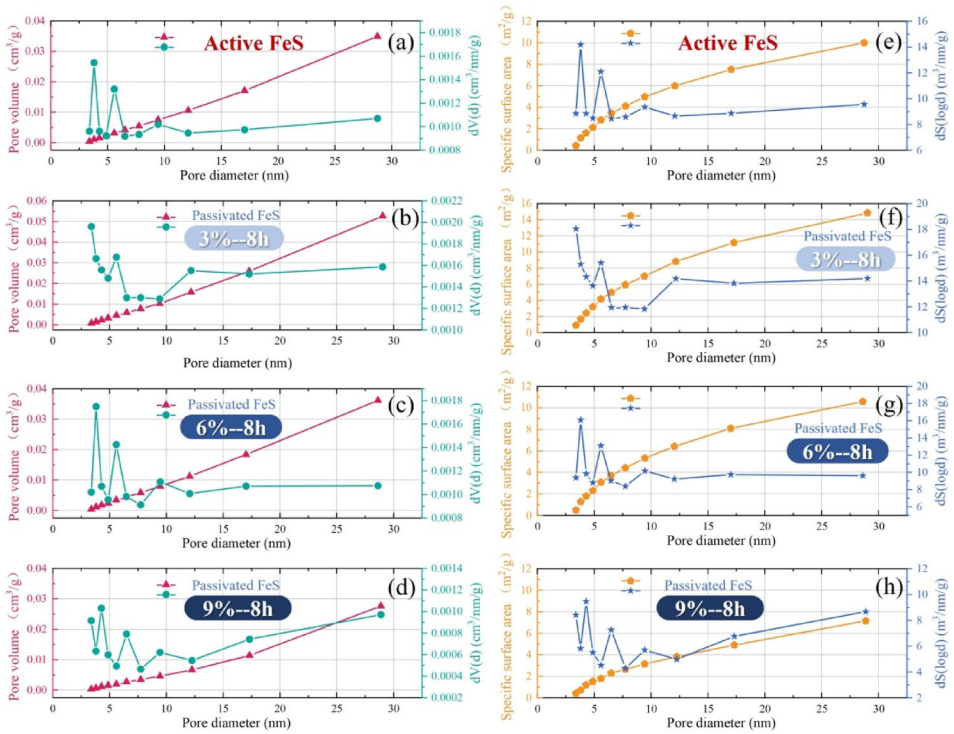

Fig. 14. The pore volume - pore diameter and pore specific surface area - pore diameter distribution diagrams of active FeS and passivated FeS samples. (**a-d**) The pore volume - pore diameter diagrams of active FeS, B8(3% passivator, 8 h), C8(6% passivator, 8 h), D8(9% passivator, 8 h). (**e-h**) The pore specific surface area - pore diameter distribution diagrams of active FeS, B8(3% passivator, 8 h), C8(6% passivator, 8 h), D8(9% passivator, 8 h).

dispersion in the growth rate of FeS pore volume, weakening the pore distribution in the microporous range. The trend of the pore area versus pore diameter curve follows a pattern similar to that of the pore volume changes.

Compared to a 3% gas-phase passivator concentration, the higher concentration facilitates a more efficient reaction between FeS and the passivator in the early stages of passivation. This rapid passivation accelerates the breakdown of the original pore structure, exposing new active surfaces that continue to passivate and form a new, more complex pore structure. As a result, the number of micropores decreases, and larger transition pores form, increasing the overall pore complexity. Therefore, with the extension of passivation time, the total pore volume and total specific surface area of passivated FeS show a decreasing trend.

For the above obtained FeS total pore volume, total specific surface area, pore diameter and other parameters, and combined with the pore size division of FeS transition pore and microporous pore parameter calculation can be obtained for this evaluation of FeS all pore parameter indicators of the specific value.

Fractal dimension calculation

To further analyze the pore roughness and adsorption capacity of reactive FeS after gas-phase passivation treatment, the Frenkel-Halsey-Hill (FHH) model is used to calculate the fractal dimension of ferrous sulfide[33–35]. The formula is shown below:

$$\ln V = Const + A \cdot \ln(\ln(P_0/P)) \tag{16}$$

$$D = A + 3 \tag{17}$$

$$D = 3A + 3 \tag{18}$$

where: V is the gas adsorption volume, $cm^3 \cdot g^{-1}$; P is the equilibrium pressure of the system, MPa; P_0 represents the saturated vapor pressure of the adsorbed gas (nitrogen) at the liquid nitrogen temperature (77 K), and the default value of this parameter is approximately 0.1Mpa; Const is a constant; A is the fractal dimension factor; D is the fractal dimension.

Generally speaking, when nitrogen adsorption is mainly dominated by van der Waals forces, the fractal dimension is calculated according to formula (18). When adsorption is mainly dominated by capillary condensation, the fractal dimension is calculated according to formula (17). However, when the absolute value of the slope A of the fractal dimension is greater than 1/3, the effect of van der Waals forces can be ignored. At a relative pressure of P/P_0 around 0.5, the adsorption capacity of active FeS increases rapidly. As the relative pressure continues to increase, the nitrogen adsorption capacity rises sharply, and the capillary condensation

phenomenon becomes more prominent, but no adsorption saturation occurs. Therefore, taking the relative pressure of 0.5 as the boundary, the surface fractal dimension D1 of FeS in the low-pressure stage and the spatial fractal dimension D2 in the high-pressure stage of nitrogen adsorption are calculated respectively, which can more effectively illustrate the influence of gas-phase passivation on the fractal characteristics of the pore structure of FeS[32].

Using a relative pressure of 0.5 as the boundary, the surface fractal dimension (D_1) and the spatial fractal dimension (D_2) are calculated from the segmented fitting slopes. The fractal dimension curve fitting of FeS obtained using the FHH model is shown in Fig. 15. A larger D_1 indicates a rougher pore surface morphology, while a larger D_2 suggests a more complex spatial structure of the pore network. Both D_1 and D_2 of FeS treated with gas-phase passivation show significant changes. Insufficient passivator concentration and shorter passivation times lead to an initial increase in the fractal dimension and pore structure complexity.

By fitting the FHH fractal dimension, the changes in the surface and spatial pore characteristics of all passivated FeS samples can be more effectively analyzed. The experimental data on the pores of ferrous sulfide is presented in the section on the experimental data from the fully automated specific surface area analyzer. Using this method, the pore characteristic parameters and fractal dimensions of ferrous sulfide can be determined under different passivator concentrations and passivation times.

Evaluation indexes and results of gas-phase passivation effect

Establishment of evaluation indicators

Evaluation indicators are an essential part in the establishment of an evaluation system. In this paper, in order to determine the passivation effect of the experimentally obtained passivated samples as the goal, the spontaneous combustion tendency of different passivated samples is determined by selecting the characteristic parameters of practical significance that can be characterized in the thermodynamic experiment and BET specific surface area measurement experiment. In order to construct the objective weights of the evaluation indexes in the subsequent entropy weight-TOPSIS evaluation process, which provides the basis for the actual comprehensive evaluation[25,36].

Thermodynamic parameter extraction

The choice of evaluation metrics is based on intuition with respect to FeS spontaneous combustion and passivation effects. From the previous analysis, the characteristic parameters that have an influential role in the FeS spontaneous combustion process are ΔG_1, ΔG_2, ΔG_3, ΔT_1, ΔT_2, ΔT_3 and the exothermic quantities Q, Q_1, Q_2, Q_3 and activation energies E, E_1, E_2, E_3, and the self-heating temperature (T_S), the ignition temperature (T_I). where ΔG_1, Q_1, and E_1 characterize the initial spontaneous combustion phase. lower $\Delta G_1/Q_1$ and higher E_1 indicate suppressed reactivity. ΔT_2 and E_3 reflect the oxygen adsorption kinetics and the high-temperature combustion energy intensity. Longer ΔT_2 and higher E_3 imply delayed combustion. T_I and T_s represent measurements of ignition delay and self-heating tendency, which are essential for spontaneous combustion assessment. Tables 2

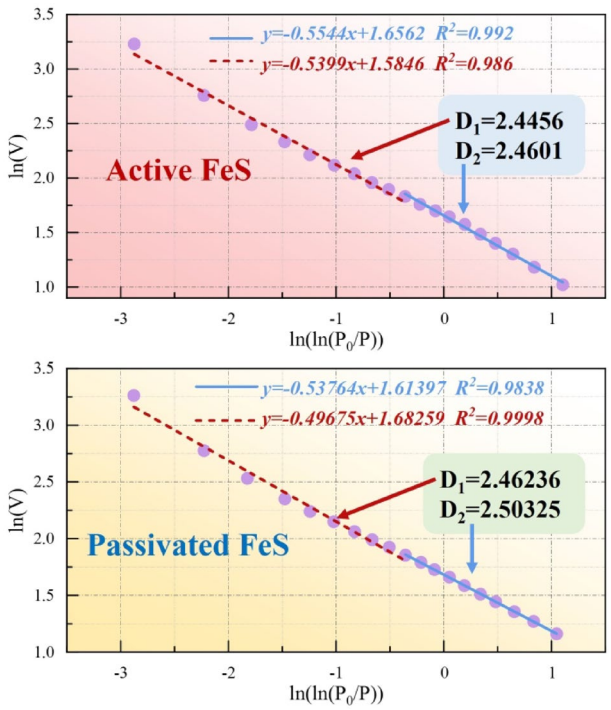

Fig. 15. The fractal dimension curve fitting of FeS obtained by FHH model.

	Evaluation parameters	ΔG_1	ΔG_2	ΔG_3	ΔT_1	ΔT_2	ΔT_3	T_S	T_I
	Unit	%	%	%	℃	℃	℃	℃	℃
Passivation degree	Indicator	-	-	+	-	-	+	+	+
3%—2 h	B2	3.22	14.76	14.77	30.14	98.21	66.94	198.30	159.97
3%—4 h	B4	3.17	13.26	13.26	35.97	97.20	69.46	202.38	159.20
3%—6 h	B6	2.70	23.69	23.68	34.49	98.24	62.57	195.93	148.62
3%—8 h	B8	5.55	11.57	11.57	32.78	97.73	56.40	200.57	142.48
6%—2 h	C2	2.91	14.25	14.25	30.16	95.13	71.65	200.37	157.14
6%—4 h	C4	1.42	15.47	15.47	32.80	96.38	71.42	200.38	155.44
6%—6 h	C6	1.41	15.54	15.54	31.43	95.14	70.87	199.51	155.82
6%—8 h	C8	0.98	12.89	12.89	28.99	92.90	65.91	198.53	155.65
9%—2 h	D2	2.55	26.43	26.43	26.06	91.74	86.70	200.32	148.02
9%—4 h	D4	1.16	21.69	21.69	30.34	85.32	87.21	204.70	158.30
9%—6 h	D6	0.72	21.86	21.86	43.70	77.47	90.70	207.90	154.40
9%—8 h	D8	0.92	19.53	19.53	48.90	44.42	92.80	203.33	149.27

Table 2. Thermodynamic characterization parameters(1).

	Evaluation parameters	Q_t	Q_1	Q_2	Q_3	E	E_1	E_2	E_3
	Unit	J/g	J/g	J/g	J/g	kJ/mol	kJ/mol	kJ/mol	kJ/mol
Passivation degree	Indicator	-	-	-	-	+	+	+	+
3%—2 h	B2	2357.52	463.11	204.87	1640.70	105.10	67.11	86.98	161.23
3%—4 h	B4	2194.99	131.90	139.71	2056.39	115.30	85.56	98.01	162.33
3%—6 h	B6	2142.10	53.88	56.35	2088.66	126.55	106.23	108.55	164.87
3%—8 h	B8	2050.37	52.23	36.55	1981.46	142.88	139.55	119.54	169.56
6%—2 h	C2	2414.55	316.23	229.89	1755.00	131.73	117.63	112.99	164.56
6%—4 h	C4	2135.39	228.12	146.14	1820.30	134.53	123.98	114.64	164.98
6%—6 h	C6	2027.65	92.41	79.44	1898.78	145.63	143.35	125.66	167.87
6%—8 h	C8	1878.14	56.23	11.15	1755.57	169.90	188.36	138.69	182.66
9%—2 h	D2	2280.11	128.88	60.05	2092.05	154.52	164.98	129.34	169.25
9%—4 h	D4	1985.02	23.00	59.00	1862.90	171.07	192.45	131.22	189.55
9%—6 h	D6	1900.81	12.32	52.68	1751.99	177.61	199.56	139.87	193.42
9%—8 h	D8	1862.10	3.56	25.92	1724.00	191.52	208.15	142.56	223.86

Table 3. Thermodynamic characterization parameters (2).

and 3 show all the thermodynamic characteristic parameters that can be used as evaluation indicators. The values are averaged over four heating rates.

Pore parameter extraction

The active and passivated FeS pore parameters obtained by the fully automated specific surface area meter can reflect the effect of gas-phase passivation on the pore characteristics of ferrous sulfide very intuitively and accurately. Therefore, the specific pore parameters obtained from the above BET specific surface area measurement experiments were characterized by feature extraction, and further endowed with objective weights and evaluated comprehensively. As shown in Fig. 16, the total pore volume, mesopore volume, and micropore volume, as well as the specific surface area values for both active and passivated iron sulfide, were determined. The fractal dimensions obtained using the FHH method were used for subsequent evaluations. The parameters considered in the microporous structure section include aperture (Ap), total specific surface area (SSA), total pore volume (V), pore volume and specific surface area of different pore diameters (V_{TP}, V_{MP}, SSA_{TP}, SSA_{MP}), surface fractal dimension D_1, and spatial fractal dimension D_2. These pore structure indicators are chosen based on their direct correlation with oxygen diffusion and reaction sites. Where smaller Ap will impede oxygen penetration and reduce reactive surface exposure. Higher SSA would correlate with greater combustion propensity due to increased reactive sites. The reduction in pore volume V after passivation implies limited oxygen accessibility. All the pore characteristic parameters available for evaluation are shown in Table 4.

Evaluation indicator correlation analysis

The characteristic parameters obtained from FeS thermodynamic experiments and BET specific surface area measurement experiments can be extracted as indicator parameters to establish correlation heat maps. The normality test was performed on the 25 sets of parameters obtained, and all the data complied with the normality test by utilizing the Shapiro-Wilk test according to the number of samples[37]. As shown in Fig. 17, correlation

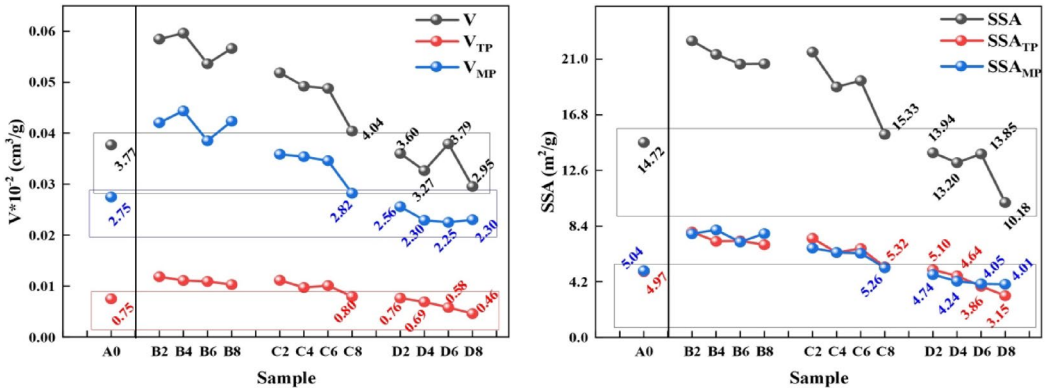

Fig. 16. The pore parameters of FeS with different pore sizes.

	Evaluation parameters	Ap	SSA	V	V_{TP}	V_{MP}	SSA_{TP}	SSA_{MP}	D_1	D_2
	Unit	nm	m^2/g	cm^3/g	cm^3/g	cm^3/g	m^2/g	m^2/g	-	-
Passivation degree	Indicator	+	-	-	+	-	+	-	-	-
3%—2 h	B2	10.44	22.39	0.058	0.012	0.042	7.95	7.82	2.48	2.47
3%—4 h	B4	11.17	21.37	0.060	0.011	0.044	7.25	8.11	2.48	2.44
3%—6 h	B6	10.40	20.63	0.054	0.011	0.039	7.28	7.20	2.49	2.47
3%—8 h	B8	10.97	20.65	0.057	0.010	0.042	7.00	7.84	2.48	2.45
6%—2 h	C2	9.63	21.54	0.052	0.011	0.036	7.48	6.74	2.49	2.49
6%—4 h	C4	10.41	18.91	0.049	0.010	0.035	6.41	6.41	2.51	2.47
6%—6 h	C6	10.07	19.38	0.049	0.010	0.035	6.70	6.35	2.52	2.48
6%—8 h	C8	10.54	15.33	0.040	0.008	0.028	5.32	5.26	2.50	2.46
9%—2 h	D2	10.34	13.94	0.036	0.008	0.026	5.10	4.74	2.47	2.47
9%—4 h	D4	9.90	13.20	0.033	0.007	0.023	4.64	4.24	2.50	2.48
9%—6 h	D6	10.95	13.85	0.038	0.006	0.022	3.86	4.05	2.51	2.45
9%—8 h	D8	11.60	10.18	0.030	0.005	0.023	3.15	4.01	2.49	2.44

Table 4. Pore characterization parameters.

analysis was used to investigate the correlations between the 25 characteristic parameters, and the Pearson correlation coefficient was used to indicate the strength of the correlations.

The color of the circle indicates that the correlation between the two indicators is either positive or negative, the darker the color, the more correlated the indicators are, and the size of the circle represents the size of the correlation coefficient value. When the absolute value of the correlation coefficient is above 0.8, it represents a strong correlation, between 0.5 and 0.8 represents a moderate correlation, between 0.3 and 0.5 represents a fair correlation, and below 0.3 represents a weak or no correlation[38].

As can be seen from the above figure, the correlation between Ap and other feature parameters is weak, but the correlation with the fractal dimension D_2 reaches 0.99, showing a very strong linear relationship. Positive correlations were found between SSA, SSA_{TP}, SSA_{MP} and the six characteristic parameters of V, V_{TP}, and V_{MP}, and the correlation coefficients showed significance. Specifically, the correlation coefficients between SSA and V_{TP} and SSA and V_{MP} were 0.98 and 0.94, respectively. The correlation coefficients between V and SSA_{TP} and SSA_{MP} were 0.94 and 0.98, and the correlations between SSA_{TP} and V_{TP}, and between SSA_{MP} and V_{MP} were almost 1. Besides, these six characteristic parameters also showed strong correlations with some parameters of thermodynamics. They show strong correlations with the four groups of activation energies E_1, E_2, E_3, E with correlation coefficients higher than 0.7, but each of them shows a negative correlation. The absolute correlation of E_1 was above 0.9. ΔG_1, ΔG_3, ΔT_1, ΔT_2, ΔT_3, Q_t, Q_1, Q_2 also have a correlation of more than 0.5 with these six sets of characteristic parameters. The correlations between the fractal dimensions D_1 and D_2 and the other parameters are weak, but the correlation coefficients between D_1 and ΔG_1 and ΔG_2 reach −0.66 and −0.62. D_2 has a correlation of 0.5 only with ΔT_1, except for a correlation coefficient of 0.99 with Ap.

In the correlation of thermodynamic parameters, ΔG_1 and ΔG_2 were positively correlated with a correlation coefficient of 0.66. The first three exothermic quantities Q_t, Q_1, Q_2 showed negative correlation with the activation energies E_1, E_2, E_3, E. Except for Ap, D_1, D_2, ΔG_1, ΔG_2, ΔG_3, Q_3, T_S, the correlation between the four groups of activation energy parameters E_1, E_2, E_3, E and other characteristic parameters was strong, and the correlation between the four groups of activation energy and other characteristic parameters was greater than 0.5. The correlation between T_I and T_S was only 0.13, which meant that there was almost no correlation between them.

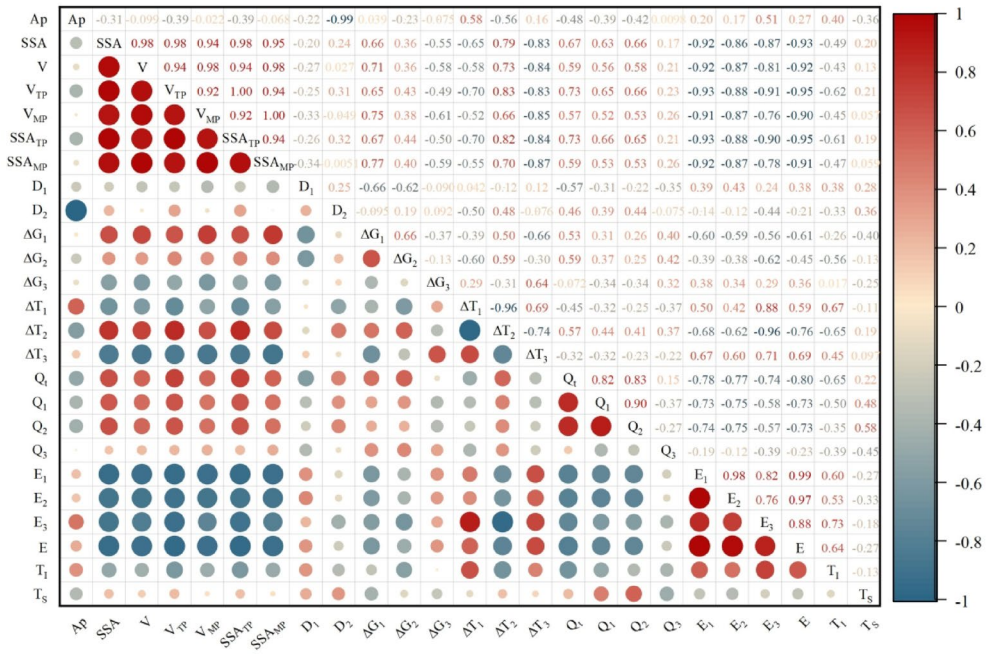

Fig. 17. Heat map of correlation between evaluation indicator parameters.

The correlation coefficients between T_I and V_{TP}, SSA_{TP}, ΔG_2, ΔT_1, ΔT_2, Q_t, Q_1, E_1, E_2, E_3, and E were − 0.62, -0.61, -0.56, 0.67, -0.65, -0.65, -0.50, 0.60, 0.53, 0.73, and − 0.64 respectively.

Regarding the correlation between pore parameters and thermodynamic parameters, the specific surface area SSA showed a strong negative correlation with the activation energy E with a correlation coefficient of -0.93. This suggests that the activation energy required for the spontaneous combustion of FeS decreases significantly with increasing SSA. Higher SSA provides more active sites for oxygen adsorption, which promotes the oxidation process and reduces the energy barrier for combustion. The pore volume V is moderately positively correlated with the amount of heat released Q, and the correlation coefficients such as Q_1, Q_2, and Q_t indicate that samples with larger pore volumes tend to release more heat during spontaneous combustion. Larger pore volume allows oxygen molecules to diffuse more rapidly into the interior of FeS, leading to more extensive oxidation reactions and higher heat release, which in turn increases its spontaneous combustion tendency characteristics.

The strong correlation between pore parameters and thermodynamic properties emphasizes the critical role of pore structure in influencing the spontaneous combustion behavior of FeS. The presence of micropores and mesopores affects both the contact of reaction sites with oxygen and the diffusion of reaction products. A higher specific surface area and larger pore volume significantly enhance the interaction between FeS and oxygen, accelerating oxidation kinetics and lowering the activation energy required for combustion. Conversely, a lower specific surface area and smaller pore volume hinder oxygen diffusion, limiting the reaction rate, which increases the activation energy and reduces the tendency for spontaneous combustion.

The changes in pore structure under different gas-phase passivation conditions are closely linked to alterations in the thermodynamic properties of FeS. Passivation treatments that lead to a significant decrease in specific surface area and pore volume generally result in higher activation energies and reduced exothermic reactions, indicating that FeS becomes more stable and less reactive. FeS samples treated with higher passivation concentrations and longer passivation times showed lower specific surface area and pore volume, accompanied by higher activation energies and diminished heat release during spontaneous combustion.

From the above analysis, there is a certain correlation between the characteristic parameters of the microporous experiments and the thermodynamic characteristic parameters, with the absolute value of the correlation coefficient of some parameters even exceeding 0.9. However, some parameters, such as Q_3 and T_S, exhibit weak or no correlation with other parameters.

Evaluation of the effect of gas-phase passivation

According to the calculation method of entropy weight method using SPSS to calculate the weights of the evaluation indexes of different passivation samples, the final objective weight values calculated by the entropy value method are shown in Table 5.

The entropy weight value represents the size of the amount of information that an indicator reflects the problem. When the more information an indicator provides, it indicates that its corresponding entropy weight value is larger, which means that the indicator can reflect the nature of the problem in a more comprehensive way. the weight values obtained from the entropy weighting method are shown in Tables 4, and the indicators with weights of more than 5% are SSA, V, ΔG_3, ΔT_2, and E_3, with weight values of 5.69%, 5.10%, 5.04%, 14.13%, 9.27%. From the perspective of pore structure, it can be seen that SSA specific surface area and V volume are

	Indicator	Information entropy e	Utility value d	Weight value ω(%)
Pore structure parameters	Aperture(Ap)	0.917	0.083	3.22
	V_{TP}	0.928	0.072	2.77
	SSA_{TP}	0.926	0.074	2.85
	SSA	0.853	0.147	5.69
	V	0.868	0.132	5.09
	V_{MP}	0.886	0.114	4.40
	SSA_{MP}	0.873	0.127	4.92
	D_1	0.928	0.072	2.78
	D_2	0.923	0.077	2.98
Thermodynamic parameters	ΔG_1	0.951	0.049	1.90
	ΔG_2	0.936	0.064	2.48
	ΔG_3	0.87	0.13	5.04
	ΔT_1	0.791	0.209	1.51
	ΔT_2	0.962	0.038	14.13
	ΔT_3	0.908	0.092	3.56
	T_I	0.912	0.088	3.42
	Ts	0.941	0.059	2.30
	Q_t	0.916	0.084	3.25
	Q_1	0.95	0.05	1.94
	Q_2	0.929	0.071	2.73
	Q_3	0.88	0.12	4.64
	E_1	0.917	0.083	3.22
	E_2	0.935	0.065	2.53
	E_3	0.76	0.24	9.27
	E	0.912	0.088	3.39

Table 5. Evaluation indicator weights.

important influencing factors, and the weights of the indicators calculated by the entropy weighting method further confirm the importance of these two indicators. For the micropores, after the oxygen adsorption process, the micropores expand to form transition pores, and the decrease in the number of micropores is more indicative of the weakening of the spontaneous combustion tendency of fes. In addition to the above parameters, the weights of other characteristic parameters are all around 2%~4%. the influence of fes.spontaneous combustion tendency does not account for a large proportion of the weight. the mechanism of inhibiting spontaneous combustion of fes.by gas-phase passivation is related to the thermodynamic behavior of fes. the passivator reacts with the active sites on the surface of fes.to form stabilized compounds, thereby reducing the availability of the active surface for oxygen adsorption. This stabilization increases the activation energy of combustion and reduces the exotherm in the early stages. As a result, the energy barrier to oxidation increases, delays the ignition temperature and mitigates self-heating. Although the altered pore structure contributes to the reduction of oxygen accessibility, the thermodynamic parameters (ΔT_1 and E_3) have a more significant effect than the microstructural metrics (SSA and V) according to the weighting, highlighting the dominant role of kinetic inhibition.

The weights of the evaluation indexes calculated by the Entropy weight method were used for TOPSIS evaluation of 12 groups of passivated samples as a way to obtain the ranking of passivation effects for different combinations of passivation concentration and passivation time. Table 6 shows the evaluation results obtained after the calculation of the TOPSIS method. The composite scores and Sort numbers of different samples were obtained through TOPSIS evaluation. This sort clearly shows the relative advantages and disadvantages of the samples under different passivation conditions. D8, D6, D4, C8, and D2 were the top five samples in the composite ranking, with composite scores of 0.743, 0.646, 0.581, 0.516, and 0.485, respectively. From the scoring results, it can be seen that the comprehensive effect of the passivated samples is not in accordance with the passivation concentration and passivation time in order to increase, such as D2 is less than C8, B8 is higher than C2 and so on. At the same passivation time, the propensity of spontaneous combustion of the samples was lower as the concentration of passivation agent increased. At the same passivate concentration, the spontaneous combustion tendency of the samples also decreases with increasing passivation time, which is in line with the preliminary verification of the thermodynamic and BET specific surface area measurement experiment. When the passivate concentration is lower at 3%, the spontaneous combustion tendency of B8 and B6 is higher than that of C2, although the passivate concentration is lower, but the increase of passivation time compensates for the defect of small passivate concentration. Compared with the proximity interpolated value of 3–6%, the proximity difference between two samples with the same passivation time is more than 0.1 in the interval of passivate concentration from 6 to 9%, and the highest difference is 0.24 between C6 and D6. Higher passivate concentration widens the gap with lower passivate concentration, and the gap between passivates increases as the passivation concentration increases. The gap between passivators also increases with the increase of passivation

Sample	positive ideal solution distance D+	Negative ideal solution distance D-	composite scores	Sort Number
B2	0.824	0.427	0.341	12
B4	0.798	0.419	0.344	11
B6	0.733	0.443	0.376	8
B8	0.762	0.441	0.366	9
C2	0.753	0.409	0.352	10
C4	0.681	0.420	0.381	7
C6	0.670	0.455	0.405	6
C8	0.558	0.596	0.516	4
D2	0.621	0.584	0.485	5
D4	0.480	0.664	0.581	3
D6	0.401	0.730	0.646	2
D8	0.314	0.907	0.743	1

Table 6. TOPSIS evaluation results.

concentration. So in the actual application process, choose 6-9% concentration of passivator will make the safety more secure.

Combined with the thermodynamic and BET specific surface area measurement experiment, the passivation time of B2, B4 and C2 samples are at a low level, the exothermic quantity is large and the spontaneous combustion tendency is high, and the active sites of adsorbed oxygen are also at a high level. For the comprehensive situation of all the samples, for the sake of safety, in the actual passivation process, we should also try to choose the passivation agent at a concentration of 6–9% and the passivation time should be higher than 4 h.

Conclusion

This study systematically evaluates the effects of different gas-phase passivation conditions on the spontaneous combustion inhibition of FeS, with a focus on analyzing the impacts of passivator concentrations (3%, 6%, 9%) and passivation durations (2–8 h) on spontaneous combustion propensity of FeS. The main conclusions are as follows:

Different concentrations (3%, 6%, 9%) and passivation durations (2–8 h) significantly influenced the spontaneous combustion inhibition of FeS. High-concentration (9%) and long-duration (8-hour) passivation treatments notably reduced both the ignition temperature and heat release of FeS. Through thermodynamic parameter analysis and BET specific surface area measurements, it was demonstrated that extended passivation durations and elevated passivator concentrations effectively decreased reactivity of FeS, thereby substantially mitigating its spontaneous combustion tendency. Gas-phase passivation modifies the surface structure of FeS, reducing its oxygen exposure and increasing the activation energy required for spontaneous ignition. The chemical reaction between passivators and active sites on FeS surfaces generates stable compounds, effectively suppressing both low-temperature and high-temperature spontaneous combustion behaviors. High-concentration and prolonged passivation not only altered FeS's microstructure but also significantly elevated the energy barrier for thermodynamic reactions, thereby delaying the spontaneous combustion process.

According to entropy weight-TOPSIS comprehensive evaluation results, FeS samples treated with 9% gas-phase passivator for 8 h demonstrated the lowest spontaneous combustion tendency, achieving a comprehensive score of 0.743, indicating optimal passivation effectiveness. In contrast, low-concentration (3%) and short-duration (2-hour) treatments showed inferior inhibition performance with a comprehensive score of 0.341. For practical safety assurance, it is recommended to employ gas-phase passivator concentrations of 6-9% with passivation durations exceeding 4 h in industrial applications. Extended treatment durations and higher passivator concentrations provide superior spontaneous combustion suppression, ensuring effective prevention of FeS ignition risks during storage and transportation in petrochemical operations.

This study has been validated under actual operating conditions in petrochemical enterprises, demonstrating practical effectiveness. However, discrepancies persist between laboratory-synthesized FeS samples and real-world industrial scenarios in terms of reaction characteristics and outcomes. Future research should integrate molecular simulations and field-collected FeS samples to systematically investigate the inhibitory effects of passivator concentration and passivation duration under authentic operational environments. Additionally, expanding the applicability assessment of gas-phase passivation across diverse operating conditions (e.g., variable temperatures, humidity levels, and sulfur content) will enhance the industrial relevance and scalability of these findings, ultimately improving security for FeS-related fire hazards in complex petrochemical infrastructures.

Environmental implication

The evaluation of FeS passivation has significant environmental implications. Passivating FeS can reduce the risk of spontaneous combustion, minimizing the release of harmful pollutants and potential environmental damage. This approach contributes to safer industrial processes and environmental protection, helping to prevent air and soil contamination. Moreover, it promotes sustainable practices by reducing the need for extensive remediation efforts in case of FeS-related incidents.

Data availability

Data is provided within the manuscript.

Received: 25 December 2024; Accepted: 16 June 2025
Published online: 01 July 2025

References

1. Dou, Z. et al. Kinetic analysis for spontaneous combustion of sulfurized rust in oil tanks. *J. Loss Prev. Process Ind.* **32**, 387–392. https://doi.org/10.1016/j.jlp.2014.10.003 (2014).
2. Bian, H., Jiang, J., Zhu, Z., Dou, Z. & Tang, B. Design and implementation of an early-stage monitoring system for iron sulfides oxidation. *Process Saf. Environ. Prot.* **165**, 181–190. https://doi.org/10.1016/j.psep.2022.07.016 (2022).
3. Liu, H. et al. Thermal decomposition kinetics analysis of the oil sludge using model-based method and model-free method. *Process Saf. Environ. Prot.* **141**, 167–177. https://doi.org/10.1016/j.psep.2020.05.021 (2020).
4. Lu, Y., Cao, X., Wang, Z. & Shen, S. Oxidative self-heating modeling of iron sulfides during the processing of high sulfur oil. *Process Saf. Environ. Prot.* **165**, 633–645. https://doi.org/10.1016/j.psep.2022.07.034 (2022).
5. Liu, H. et al. Thermodynamics and Inhibition mechanism of imidazolium-based ionic liquids for inhibiting spontaneous combustion of iron sulfide. *Fuel* **338**, 127335. https://doi.org/10.1016/j.fuel.2022.127335 (2023).
6. Dou, Z. et al. Oxidizing-gas-based passivation of pyrophoric iron sulfides. *Chem. Eng. Commun.* **208**, 1395–1404. https://doi.org/10.1080/00986445.2020.1783538 (2021).
7. Gao, J. et al. Mechanism of gas-phase passivation Inhibition during FeS self-ignition based on pore structure and fractal characteristics. *Fuel* **357**, 129839. https://doi.org/10.1016/j.fuel.2023.129839 (2024).
8. Xu, Q. et al. Spontaneous combustion characteristic stages of active FeS and its Inhibition effect by Gas-Phase passivation. *Combust. Sci. Technol.* 1–17. https://doi.org/10.1080/00102202.2023.2177511 (2023).
9. Denney, D. FeS-Scale cleanout with High-Pressure coiled tubing and tailored fluid. *J. Petrol. Technol.* **66**, 154–156. https://doi.org/10.2118/0914-0154-JPT (2015).
10. Chiriță, P. Aqueous oxidation of Iron monosulfide (FeS) by molecular oxygen. *Miner. Process. Extr. Metall. Rev.* **37**, 305–310. https://doi.org/10.1080/08827508.2016.1218866 (2016).
11. Gao, J. C., Man, X. M., Shen, J., Meng, Q. Q. & Zhou, S. Y. Synthesis of pyrophoric active ferrous sulfide with oxidation behavior under hypoxic conditions. *Vacuum* **143**, 386–394. https://doi.org/10.1016/j.vacuum.2017.07.001 (2017).
12. Wang, X., Wang, L., Li, W. & Liu, D. Experimental and simulation study of inert gas mixture inhibiting coal spontaneous combustion. *Sci. Rep.* **14**, 4305. https://doi.org/10.1038/s41598-024-53979-0 (2024).
13. Onawole, A. T., Hussein, I. A., Nimir, H. I., Ahmed, M. E. M. & Saad, M. A. Molecular design of novel chemicals for Iron sulfide scale removal. *J. Chem.* **2021** (7698762). https://doi.org/10.1155/2021/7698762 (2021).
14. Yang, R. et al. Cause analysis and prevention measures of fire and explosion caused by sulfur corrosion. *Eng. Fail. Anal.* **108**, 104342. https://doi.org/10.1016/j.engfailanal.2019.104342 (2020).
15. Shi, L., Shuai, J. & Xu, K. Fuzzy fault tree assessment based on improved AHP for fire and explosion accidents for steel oil storage tanks. *J. Hazard. Mater.* **278**, 529–538. https://doi.org/10.1016/j.jhazmat.2014.06.034 (2014).
16. Hasanzadeh, R. et al. Decision analysis for plastic waste gasification considering energy, exergy, and environmental criteria using TOPSIS and grey relational analysis. *Process Saf. Environ. Prot.* **174**, 414–423. https://doi.org/10.1016/j.psep.2023.04.028 (2023).
17. Hoseinpour, M., Sadrnia, H., Tabasizadeh, M. & Ghobadian, B. Evaluation of the effect of gasoline fumigation on performance and emission characteristics of a diesel engine fueled with B20 using an experimental investigation and TOPSIS method. *Fuel* **223**, 277–285. https://doi.org/10.1016/j.fuel.2018.02.044 (2018).
18. Fahmi, A., Khan, A., Thabet, A. & Alqudah, M. A. Natural gas based on combined fuzzy TOPSIS technique and entropy. *Heliyon* **10**, e23391. https://doi.org/10.1016/j.heliyon.2023.e23391 (2024).
19. Tüysüz, N. & Kahraman, C. An integrated picture fuzzy Z-AHP & TOPSIS methodology: application to solar panel selection. *Appl. Soft Comput.* **149**, 110951. https://doi.org/10.1016/j.asoc.2023.110951 (2023).
20. Zhu, S. B. et al. Evaluating the application potential of Acid-Modified cotton straw biochars in alkaline soils based on entropy weight TOPSIS. *Agronomy-Basel* **13**, 2807. https://doi.org/10.3390/agronomy13112807 (2023).
21. Wu, J., Zhao, G., Wang, N., Xu, Y. & Wang, M. Research on optimization of mining methods for broken ore bodies based on interval-valued pythagorean fuzzy sets and TOPSIS-GRA. *Sci. Rep.* **14**, 23397. https://doi.org/10.1038/s41598-024-73814-w (2024).
22. Lourenzutti, R. & Krohling, R. A. A generalized TOPSIS method for group decision making with heterogeneous information in a dynamic environment. *Inf. Sci.* **330**, 1–18. https://doi.org/10.1016/j.ins.2015.10.005 (2016).
23. Yoon, K. P. & Kim, W. K. The behavioral TOPSIS. *Expert Syst. Appl.* **89**, 266–272. https://doi.org/10.1016/j.eswa.2017.07.045 (2017).
24. Li, Y. et al. Distribution of geothermal resources in Eryuan County based on entropy weight TOPSIS and AHP–TOPSIS methods. *Nat. Gas Ind. B.* **11**, 213–226. https://doi.org/10.1016/j.ngib.2024.03.002 (2024).
25. Pandey, V., Dincer, H. & Komal & A review on TOPSIS method and its extensions for different applications with recent development. *Soft Comput.* **27**, 18011–18039. https://doi.org/10.1007/s00500-023-09011-0 (2023).
26. Makwakwa, T. A., Moema, D., Nyoni, H. & Msagati, T. A. M. Ranking of dispersive-extraction solvents pairs with TOPSIS for the extraction of mifepristone in water samples using dispersive liquid-liquid Microextraction. *Talanta Open.* **7**, 100206. https://doi.org/10.1016/j.talo.2023.100206 (2023).
27. Liu, H. et al. Evaluation of the spontaneous combustion tendency of corrosion products in oil tanks based on TOPSIS methodologies. *J. Loss Prev. Process Ind.* **71** https://doi.org/10.1016/j.jlp.2021.104475 (2021).
28. Xiang, C. L. et al. Thermodynamic model and kinetic compensation effect of spontaneous combustion of sulfur concentrates. *Acs Omega.* **5**, 20618–20629. https://doi.org/10.1021/acsomega.0c02884 (2020).
29. Guo, X., Fu, H., Gao, X., Zhao, Z. & Hu, Z. Study on the adsorption of Zn(II) and Cu(II) in acid mine drainage by fly Ash loaded nano-FeS. *Sci. Rep.* **14**, 9927. https://doi.org/10.1038/s41598-024-58815-z (2024).
30. Li, B., Shi, Z., Wang, Z. & Huang, L. Effect of liquid nitrogen Freeze-Thaw cycles on pore structure development and mechanical properties of coal. *ACS Omega.* **7**, 5206–5216. https://doi.org/10.1021/acsomega.1c06296 (2022).
31. Fan, L. et al. Pore structure evolution and fractal analysis of Shenhua non-caking coal during low-temperature oxidation. *Energy Sour. Part A Recover. Utilization Environ. Eff.* **44**, 6856–6867. https://doi.org/10.1080/15567036.2022.2103213 (2022).
32. Bu, Y. et al. Study on pore structure change and lean oxygen re-ignition characteristics of high-temperature oxidized water-immersed coal. *Fuel* **323**, 124346. https://doi.org/10.1016/j.fuel.2022.124346 (2022).
33. Wang, H., Li, J., Zhang, Y., Wu, Y. & Wang, Z. Study on the evolution of the pore structure of low rank coal during spontaneous combustion. *Environ. Sci. Pollut Res. Int.* https://doi.org/10.1007/s11356-022-25069-z (2023).
34. Turlapati, V. Y., Prusty, B. K. & Bakshi, T. Detailed pore structure study of Damodar Valley and upper Assam basin shales using fractal analysis. *Energy Fuels.* **34**, 14001–14011. https://doi.org/10.1021/acs.energyfuels.0c02785 (2020).
35. Anand, A., Balikram, A. & Ojha, K. Evaluation of pore characteristics of deeper Cambay shale under simulated pre/postsorption conditions by CH4 and CO2 gases. *Energy Fuels.* **37**, 16536–16550. https://doi.org/10.1021/acs.energyfuels.3c02917 (2023).

36. Li, X. et al. Application of the entropy weight and TOPSIS method in safety evaluation of coal mines. *Procedia Eng.* **26**, 2085–2091. https://doi.org/10.1016/j.proeng.2011.11.2410 (2011).
37. Zhou, Y., Zhang, Q., Singh, V. P. & Xiao, M. Z. General correlation analysis: a new algorithm and application. *Stoch. Env. Res. Risk Assess.* **29**, 665–677. https://doi.org/10.1007/s00477-014-0970-8 (2015).
38. Khan, M. M. H., Rafii, M. Y., Ramlee, S. I., Jusoh, M. & Al Mamun, M. Path-coefficient and correlation analysis in Bambara groundnut (Vigna subterranea [L.] Verdc.) accessions over environments. *Sci. Rep.* **12**, 245. https://doi.org/10.1038/s41598-021-03692-z (2022).

Acknowledgements
The authors are grateful to the Science and Technology Research Project of the Educational Department of Liaoning Province for providing the financial support.

Author contributions
Y.Z. and L.Z. was involved in conceptualization; Y.Z. and H.K. was involved in methodology; R.H. and Q.X. was involved in testing; Y.Z. and Q.X. was involved in validation; H.K. and L.Z. was involved in resources; Y.Z. and R.H. wrote the original draft; H.K. and Q.X. was involved in writing—review and editing; L.Z. was involved in funding acquisition;

Funding
This work was funded by the Science and Technology Research Project of the Educational Department of Liaoning Province (NO. JYTQN2023346).

Declarations

Competing interests
The authors declare no competing interests.

Additional information
Correspondence and requests for materials should be addressed to Y.Z. or H.K.

Reprints and permissions information is available at www.nature.com/reprints.

Publisher's note Springer Nature remains neutral with regard to jurisdictional claims in published maps and institutional affiliations.